Segmentation of Medical Image Sequence under constraints: Application to Non Invasive Assessment of Pulmonary Arterial Hypertension:

Running title: Image segmentation under interpolation conditions.

Authors: Dominique Apprato*, Dominique Ducassou♦, Christian Gout§, Eric Laffon♦,♯, Carole Le Guyader§.

Complete affiliation:

§ INSA de Rouen, Laboratoire de Mathématiques de l'INSA, Place Emile Blondel, BP 08, 76 131 Mont-Saint-Aignan cedex, France.

♦Service de Médecine Nucléaire, Hôpital du Haut-Lévêque, Avenue de Magellan, 33600 Pessac, France

♯Laboratoire de Physiologie Cellulaire Respiratoire, INSERM EMI 0356, Université Victor Segalen Bordeaux 2, Bordeaux, France.

∗ Université de Pau, Département de Mathématique, 64 000 Pau, France.

dominique.apprato@univ-pau.fr
medecine-nucleaire.ducassou@chu-bordeaux.fr>
chris_gout@cal.berkeley.edu
elaffon@u-bordeaux2.fr
carole.leguyader@laposte.net

Abstract: In this paper, we propose a new segmentation model including geometric constraints, namely interpolation conditions, to detect objects in a given image sequence. We propose to apply the deformable models to an explicit function to avoid the problem of parameterization (see Gout and Vieira-Testé [13]). A problem of energy minimization on a closed subspace of a Hilbert space is defined and introducing Lagrange multipliers enables us to formulate the corresponding variational problem with interpolation conditions. We apply this method in order to ouline the cross-sectional area of a great thoracic vessel, namely the main pulmonary artery, in order to non invasively assess pulmonary arterial hypertension (see Laffon et al. [16], [15] and [14] for more details).

Key words *:* Segmentation, deformable models, energy minimization, level set method, PDE.

CRC (1998): **I.4.6, G.1.2 & G.1.8.**

Acknowledgements

This work was supported in part by CHU of Bordeaux (grant from "appel d'offre interne 2000" n°01-06).

1 Introduction

Segmentation processing is a crucial step in image analysis (Sonka & *al.* [23]). It consists mainly in detecting and visualizing the common boundaries of distinct objects in the image. A survey of segmentation methods can found in Gout and Vieira-Testé [13]. Two kinds of problems remain currently encountered in segmentation using deformable models (Terzopoulos et al. [24]) :

1. Firstly, issues linked to the model and, to be more precise, to the parameterization. Indeed, parameterization does not allow for topological changes, which is annoying when there are several objects to detect. It does not allow either for cusps and corners, a case that is encountered when there are triple points, when the curve is supposed to be a connected curve, etc... It means that the final curve will have the same topology as the initial contour. Besides, as mentioned by Caselles et *al.* [2], this approach is also non intrinsic since the energy depends on the parameterization of the curve and is not directly related to the object geometry.

2. Secondly, issues linked to the image itself. For instance, segmentation is hard to handle when some image data are missing or when some regions are homogeneous. We can also have *a priori* knowledge on our image, that is to say interpolation conditions that have to be integrated in the segmentation process. In geophysical fields for example, well data that correspond to the interface between two different layers may be given. The segmentation process enables us to isolate the various layers of the ground and thus these *well data* are exactly interpolation conditions. This should be taken into account in the model under study. Previous work has been made in this direction by Vieira-Testé [25] or Apprato et al. [1] with the classical deformable models and parameterization was here again a real hindrance, particularly in the parameterization of interpolation conditions.

In this paper, we propose a new approach : to sort out the issue of parameterization, we use a Level Set approach, developed by Osher & Sethian [22]. Instead of working with a parameterized curve Γ, we represent it implicitly via an explicit function Φ. Γ is the zero Level Set of the function Φ, ie $\Gamma = \{(x, y), \Phi(x, y) = 0\}$ and the evolution of the curve is given at any time t by the zero Level Set of $\Phi(x, y, t)$.
Besides, the interpolation conditions are integrated in our model. If some image data are missing, defining geometrical constraints helps the contour to evolve towards the outlines of the object to detect. These interpolation conditions play the same role as the pushing force of the Balloon Model. If *a priori* knowledge of the image is given, it is fully taken into account in our model.
So, in our model, we propose to apply the Deformable Models (Cohen, Cohen, and Ayache [7], Cohen, Bardinet and Ayache [9]) to an explicit function Φ instead of a parameterized curve Γ. Then, we will generate our curve, taking the zero Level Set of the surface. The different steps of the presentation are the following ones : in section 2, we make an accurate depiction of our modelling. The Level Set approach forces us to work in a space of higher dimension. We will see how to handle this property. In section 3, we will mainly focus on the mathematical framework. That section is divided into 3 parts. First, we define our problem of non-convex functional minimization on a Hilbert space.

Then, the interpolation constraints lead us to solve this problem on a closed vector subspace of this Hilbert space. The Lagrange multipliers (Ciarlet [4]) enable us to formulate the variational problem. Section 4 is devoted to the discretization of the problem which is done with finite elements for space discretization and implicit finite differences scheme for time discretization.
In section 5 experimental results with the proposed approach are given in a medical imaging framework. Medical imaging can no longer be considered only as morphological imaging, it has become functional, and nowadays physicians have to quantify parameters. Magnetic resonance imaging (MRI) is a non invasive medical imaging technique, hence repetitive, which has recently allowed for the assessment of pressure values at the level of the main pulmonary artery (MPA) in patients suspected of pulmonary arterial hypertension (see Laffon et al. [16], [15] and [14]). That assessment requires both blood flow velocity and vessel cross-sectional area (CSA) measurements, throughout the cardiac cycle, which can be carried out by means of velocity-encoded sequences (see Laffon et al. [14]). In old patients, suffering from breathlessness, the data acquisition cannot be performed in an optimal manner, which can lead to some images of the frame in which the MPA CSA cannot be clearly identified in its whole. However, in those images, the physician who manually outlines the vessel wall, reasonably assumes a circle-like outlining over the unclear parts of the vessel wall. In other words, the physician interpolates with *a priori* knowledge, since it is reasonable to assume that a vessel CSA exhibits an anatomical round shape. Nevertheless, although they are reasonable, such assumptions lead to intra and inter-observer variability, and consequently to uncertainty in pressure estimations in a given patient. The difficulty of this vessel outlining exactly matches the issue raised in Fig. 1, which has been addressed in the present work

2 The Data

We have a sequence of images: an example can be found on the web at URL http://www.univ-pau.fr/~cgout/chubdx/index1.htm.

Figure 1 refers to a slice set perpendicularly to the MPA axis (arrow) of a 78 year old patient. This patient was suspected of pulmonary arterial hypertension, suffering from breathlessness. The presented magnitude image was acquired from a velocity encoded sequence (Venc = 1.5 m/s), during a 5 min time duration, with a 30 ms temporal resolution (1 Tesla Magnetom Expert imager; Siemens; Germany). The image quality is moderate, and in particular the vessel wall is irregular around the arrow, that is not anatomically possible, and therefore an interpolation in the outlining by the physician is needed. Impairement in the contrast between the vessel blood and the surrounding medium can be related to (i) partial volume effect, that is observed in particular at the level indicated by the arrow (beginning of the right pulmonary artery), (ii) flow turbulences, that are correlated with the severity of the pulmonary arterial hypertension, (iii) the absence of the so-called "proton inflow phenomenon", which leads to poor blood images contrast at the end-diastolic cardiac phase in the image frame (19, 20). It should be noted that very recent MR imagers (1.5 Tesla imagers) might allow to perform similar acquisition within a 30 s-breathhold (segmented velocity-encoded acquisition, Venc = 1.5 m/s, 39 ms temporal resolution), leading to better quality images. Nevertheless, (i) unclear parts of the MPA wall will still remain around the MPA CSA at the end-diastolic cardiac phase, (ii) as presented in Fig. 1, patients suffering from pulmonary arterial hypertension are usually

unable to perform a 30s-breathhold.

Figure 1: The arrow indicates the part of the contour which implies the requirement of interpolation data in the segmentation process because of the non sufficient quality of the contrast in this zone.

From a more theoretical point of view, we define an image as it follows. Let Ω be a bounded open subset of $\Re^2$. Let us denote by I our given image,

$$I = \begin{cases} \Omega \to \Re \\ (x,y) \mapsto I(x,y) \end{cases} .$$

The use of the Level Set approach in our modelling implies that we work in a space of higher dimension. We need, therefore, to build a 3D image. This image $\tilde{I}$ is defined as follows :

$$\tilde{I} = \begin{cases} \Omega \times \Re \to \Re \\ (x,y,z) \mapsto \tilde{I}(x,y,z) \\ \text{such that, } \forall (x,y) \in \Omega, \tilde{I}(x,y,0) = I(x,y). \end{cases}$$

We just impose that for the value $z = 0$, $\tilde{I}$ coincides with the initial image I. The image $\tilde{I}$ is the superimposition of I:

$$\tilde{I} = \begin{cases} \Omega \times \Re \to \Re \\ (x,y,z) \mapsto \tilde{I}(x,y,z) \\ \text{and } \forall (x,y) \in \Omega, \forall z \in \Re, \tilde{I}(x,y,z) = I(x,y). \end{cases}$$

By this process, we aim at getting the singularities of I (we mean $\|\nabla I\| \simeq +\infty$) thanks to the singularities of $\tilde{I}$. At each time $t \in [0,T]$, the function Φ will segment $\tilde{I}$ and the zero level set of Φ, denoted by Γ, will segment I.

Furthermore, *a priori* knowledge of interpolation conditions leads to some geometric constraints on the model under study. We denote by $P = \{a_1, a_2, .., a_N\}$ a set of N distinct points to interpolate that we assume to be included in the set of singularities of I.

$$\forall i \in \{1, ..., N\}, a_i = (x_i, y_i) \in \Omega.$$

The points of P have to belong to the zero Level Set Γ of Φ (interpolation conditions), so,

$$\forall i \in \{1, ..., N\}, \Phi(a_i) = \Phi(x_i, y_i) = 0.$$

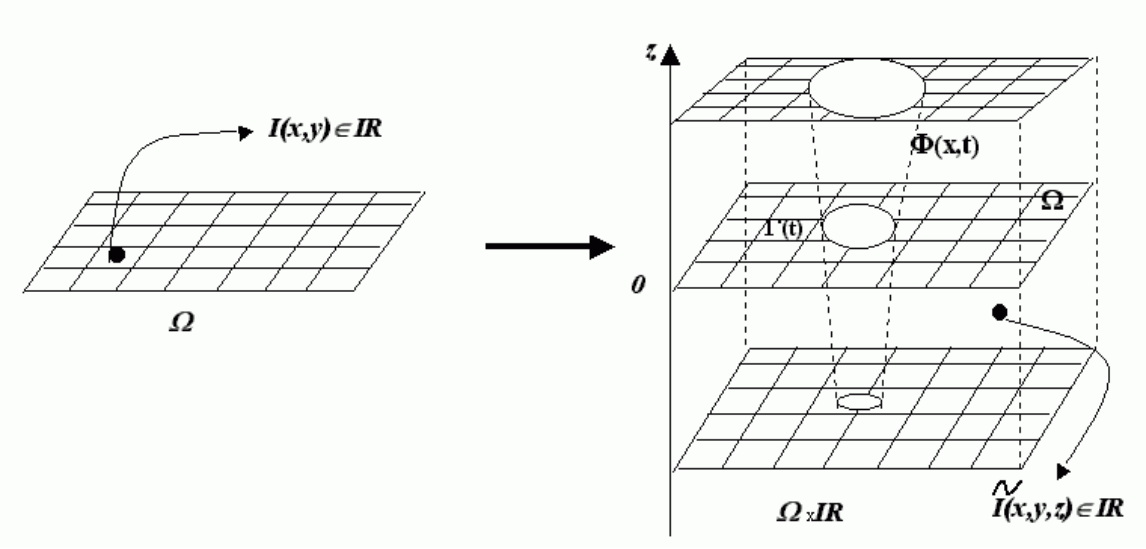

Figure 2: *Left:* Initial image. *Right:* construction of the 3D image.

3 Mathematical Modelling

3.1 Energy minimization problem

As mentioned in section 1, we define an energy minimization problem on a space of acceptable representations. We take

$$V = H^2(\Omega) \tag{1}$$

as our space of acceptable representations, where $H^2(\Omega)$ is the usual Sobolev space on Ω. The interpolation conditions must be taken into account in our stationary space of acceptable representations. Let us denote by K the vector subspace of V defined by $K = \{v \in V, \beta(v) = 0\}$, where β is the linear mapping defined by :

$$\beta : v \in V \mapsto \beta(v) = (v(a_i))_{i\in\{1..N\}} \in (\Re)^N . \tag{2}$$

The linear form β is continuous on V since $H^2(\Omega) \circlearrowleft C^0(\overline{\Omega})$. Clearly, K is a closed subspace of V since $K = Ker\,\{\beta\}$.

The deformable models consist in attracting a representation towards the singularities of a given image I. The representation responds naturally to applied forces :

1. internal forces which describe the properties of elasticity and rigidity of the representation. Formally, it is linked to the first and second derivatives.

2. external forces derived from a potential function which attracts the representation towards the singularities of the image $\widetilde{I}$. The potential function is chosen such that it tends to its minimum when the representation is located at the points of maxima $\left\|\nabla\widetilde{I}\right\|$.

For the criterion linked to internal forces, for any $v \in V$, we define the internal energy (*regularization energy*) E_{int} by

$$E_{int}(v) = \int_\Omega \epsilon_1(x,y)[(\frac{\partial v(x,y)}{\partial x})^2 + (\frac{\partial v(x,y)}{\partial y})^2] + \epsilon_2(x,y)[(\frac{\partial^2 v(x,y)}{\partial x^2})^2 + 2(\frac{\partial^2 v(x,y)}{\partial x \partial y})^2 + (\frac{\partial^2 v(x,y)}{\partial y^2})^2]dxdy \quad . \tag{3}$$

This energy is dictated by two parameters of control: ϵ_1 is the elasticity parameter and ϵ_2 the rigidity parameter. If we increase ϵ_1, we tend to eliminate the loops and ripples of the surface (see for instance ([20])). In experimental examples, we consider ϵ_1 and ϵ_2 constant on Ω.

For the criterion linked to external forces, for any $v \in V$, we define the external energy E_{ext} by

$$E_{ext}(v) = \int_\Omega P(x,y,v(x,y))dxdy. \tag{4}$$

with P the potential function expressed with the gradient of the image $\tilde{I}$. The following expression is often given for P (see for instance [23]):

$$P(x,y,z) = -\alpha||\nabla \tilde{I}(x,y,z)||^2, \alpha > 0, \tag{5}$$

but we can also find (see for instance [17]):

$$P(x,y,z) = \frac{\alpha}{1 + ||\nabla \tilde{I}(x,y,z)||^2}, \alpha > 0, \tag{6}$$

where $\|\cdot\|$ denotes the Euclidean norm. With these notations, we define the functional E on V such that

$$\begin{cases} \forall v \in V, \\ E(v) = E_{int}(v) + E_{ext}(v) \end{cases} . \tag{7}$$

We denote by a the following bilinear form associated to the functional E_{int} defined on $V \times V$:

$$\begin{cases} a : (u,v) \mapsto a(u,v) \in \Re, \\ a(u,v) = \\ \int_\Omega \epsilon_1(x,y)[(\frac{\partial u}{\partial x})(\frac{\partial v}{\partial x}) + (\frac{\partial u}{\partial y})(\frac{\partial v}{\partial y})] + \epsilon_2(x,y)[(\frac{\partial^2 u}{\partial x^2})(\frac{\partial^2 v}{\partial x^2}) + 2(\frac{\partial^2 u}{\partial x \partial y})(\frac{\partial^2 v}{\partial x \partial y}) + (\frac{\partial^2 u}{\partial y^2})(\frac{\partial^2 v}{\partial y^2})]dxdy \end{cases} .$$

Thus E can be rewritten by

$$\begin{cases} \forall v \in V, \\ E(v) = a(v,v) + E_{ext}(v) \end{cases} . \tag{8}$$

Remark that a is a continuous bilinear form on $V \times V$. We formulate the problem of minimization as follows:

$$\begin{cases} \text{Find} \quad \Phi \in K, \forall v \in K, \\ E(\Phi) \leq E(v) \end{cases} . \tag{9}$$

It is a non-linear problem of minimization on the vector subspace K of V that includes the geometric constraints. The non-linearity stems from the non-linearity of the potential P.

3.2 Evolution problem

We have considered the problem of energy minimization as a static problem. The potent of deformable models is to introduce a dynamic term in the functional we want to minimize. The model evolves according to time t until it reaches its equilibrium. The stationary state is then established and the surface no longer evolves. So now, we assume that Φ is a function of the variables x, y and t. The dynamic component added to the functional is defined by:

$$\frac{1}{2}\frac{\partial}{\partial t}\int_{\Omega}\epsilon(x,y)(\Phi(x,y,t))^2 dxdy.$$

with a parameter of control ϵ with respect to the L^2 norm of Φ for space. The parameter ϵ controls the deformation of the surface. The more we increase ϵ, the less the model is deformed. In experimental examples, we will consider ϵ constant on Ω.
We now reformulate our energy minimization problem, that is now an evolution problem. Let V be the space defined in (1) equipped with the scalar product $((.,.))$ and the associated norm $||.||$, we denote by $W(]0,T[,V)$ the following space:

$$W(]0,T[,V) = \left\{ \; u \in L^2(]0,T[,V) \text{ such that } \frac{du}{dt} \in L^2(]0,T[,V') \; \right\},$$

where V' is the dual of V. The Hilbert space $W(]0,T[,V)$ is equipped with the scalar product:

$$(u,v)_{W(]0,T[,V)} = \int_0^T ((u(t),v(t)))dt + \int_0^T \left(\frac{du(t)}{dt}, \frac{dv(t)}{dt}\right)_{V'} dt,$$

and with the associated norm

$$|u|_{W(]0,T[,V)} = (u,u)^{1/2}_{W(]0,T[,V)}.$$

The evolution problem associated with the problem (9) is then given by

$$\left\{ \begin{array}{l} \text{Find } \Phi \in W(]0,T[,V), \\ \forall t \in]0,T[, \Phi(t) \in K, \\ \forall w \in W(]0,T[,V), w(t) \in K \text{ for } \; t \in]0,T[, \\ J(\Phi) \leq J(w), \\ \Phi(.,.,0) = \Phi_0 \in L^2(\Omega), \end{array} \right. \tag{10}$$

where the functional J is defined by

$$J(w) = \frac{1}{2}\frac{\partial}{\partial t}\int_{\Omega}\epsilon(x,y)(w(x,y,t))^2 dxdy + E(w).$$

In the discretization stage of our study, we approximate the space V by the space V_h. One could think of including the geometrical constraints in the definition of V_h but we did not want to link the interpolation conditions and the space of approximation.
The variational formulation of our problem is obtained with the use of Lagrange multipliers (Ciarlet [4]). Then, the problem (10) implies the following one

$$\left\{ \begin{array}{l} \text{Find } \Phi \in W(]0,T[,V), \\ \forall t \in]0,T[, \Phi(t) \in K \\ \forall w \in W(]0,T[,V), w(t) \in K \text{ for } \; t \in]0,T[, \\ J'_{\Phi}(w) = 0. \\ \Phi(.,.,0) = \Phi_0 \in L^2(\Omega). \end{array} \right.$$

3.3 Variational formulation

Let us evaluate the Gâteaux derivative of J at Φ in the direction v

$$J'_{\Phi}(v) = lim_{h\to 0}\frac{J(\Phi+hv)-J(\Phi)}{h}.$$

We get:

$$\begin{array}{rl} J'_{\Phi}(v) = & \frac{d}{dt}\int_{\Omega}\epsilon(x,y)\Phi v dxdy + \int_{\Omega}\epsilon_1(x,y)[2\frac{\partial\Phi}{\partial x}\frac{\partial v}{\partial x}+2\frac{\partial\Phi}{\partial y}\frac{\partial v}{\partial y}]dxdy \\ & + \int_{\Omega}\epsilon_2(x,y)[2\frac{\partial^2\Phi}{\partial x^2}\frac{\partial^2 v}{\partial x^2}+4\frac{\partial^2\Phi}{\partial x\partial y}\frac{\partial^2 v}{\partial x\partial y}+2\frac{\partial^2\Phi}{\partial y^2}\frac{\partial^2 v}{\partial y^2}]dxdy \\ & + \int_{\Omega}\frac{\partial P}{\partial z}(x,y,\Phi(x,y,t))v dxdy. \end{array}$$

We get the variational formulation of our problem taking as test function, v, on the stationary space V for any $t\in]0,T[$ and using Lagrange multipliers, we obtain the following problem:

$$\left\{\begin{array}{l} \text{Find } (\Phi,\lambda)\in W(]0,T[,V)\times\mathcal{F}([0,T],\Re^N), \\ \forall t\in]0,T[,\Phi(t)\in K \\ \forall v\in V: \\ \int_{\Omega}\epsilon(x,y)\frac{\partial\Phi}{\partial t}v dxdy + 2a(\Phi(t),v) \\ \\ + \int_{\Omega}\frac{\partial P}{\partial z}(x,y,\Phi(x,y,t))v dxdy + <\lambda(t),\beta(v)>_N = 0, \\ \text{with} \\ \Phi(.,.,0)=\Phi_0\in L^2(\Omega), \lambda(0)=\lambda_0\in\Re^N, \end{array}\right. \tag{11}$$

where $\mathcal{F}([0,T],\Re^N)$ is the space of functions from $[0,T]\to\Re^N$, and where $<.,.>_N$ is the inner product on $\Re^N$. This formulation of the problem with Lagrange multipliers enables us to solve an equation on the space V instead of solving an equation on a closed subspace of V.
The discretization is given in Le Guyader et al. [17]. We use classical schemes: finite differences (see Euvrard [11] for more details) on time and finite elements (see Ciarlet [5], Gout [12] for more details) on space.

4 Numerical results

We choose the potential defined in (6). Parameters introduced in our model are considered constant on Ω. The values of ϵ_1 and ϵ_2 were chosen so as to bestow the same weight to internal and external forces. For the estimation of these parameters, we have followed Cohen's results [6] and have used a mere discretization with a finite differences method of E_{int}. It enables us to take

$$\left\{\begin{array}{l} \epsilon = 1, \\ \epsilon_1 \simeq h_x^2, \\ \epsilon_2 \simeq h_y^4, \\ \Phi_0(x,y) = \dfrac{\left((x-48.5)^2+(y-61.5)^2-25^2\right)}{1000}, \\ \delta t = 0.001. \end{array}\right.$$

We obtain the following result.

The MPA CSA variations versus time, throughout a cardiac cycle, obtained from the present automatic segmentation method are in agreement with previous results obtained

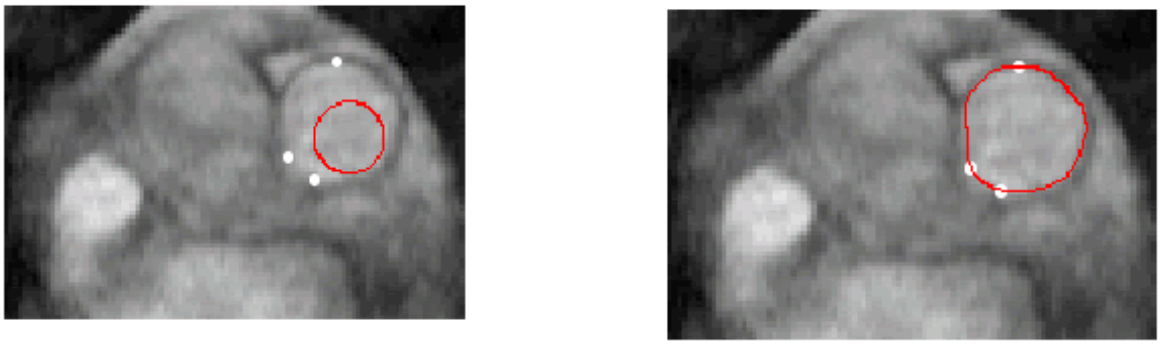

Figure 3: This is a zoom of the zone to segment taken from Figure 1. **Left**: the initial condition with 3 interpolation conditions: the two interpolation conditions (at the bottom on the left) help the segmentation process on a zone where the contrast is not good while the third interpolation condition -top of the MPA- allows us to take an initial condition which is as far as we want from the final result. **Right**: the final result.

from a manual outlining (see Laffon et al. [14], [15] and [16]). Moreover, the present method enables us to get a reliable assessment of the systolic-diastolic difference in the vessel CSA, which should lead to a further improvement in the accuracy of a non invasive blood pressure estimation, as discussed in details in a recently published paper by Laffon et al. [14].

The complete sequence after the segmentation process can be found at URL : http://www.univ-pau.fr/~cgout/chubdx/index1.htm.

References

[1] D. Apprato, J.B. Betbeder, C. Gout, S. Vieira-Testé, A Segmentation method under Geometric Constraints and after Pre-processing, Curves and Surfaces IV, A. Cohen, C. Rabut and L. L. Schumaker eds, Vanderbilt University Press, Nashville, pp. 9-18, 1999.

[2] V. Caselles, R. Kimmel, G. Sapiro, Geodesic Active Contours, International Journal of Computer Vision 22(1), 61-79, 1997.

[3] V. Caselles, F. Catté, T. Coll, F. Dibos, A geometric model for active contours in image processing, Numerische Mathematik 66, 1-31, 1993.

[4] P.G. Ciarlet, Introduction à l'analyse matricielle et à l'optimisation, Masson, Paris, 1985.

[5] P.G. Ciarlet, The finite element method for elliptic problems, North-Holland, Amsterdam, 1987.

[6] I. Cohen, Modèles déformables 2D et 3D: application à la segmentation d'images médicales, thèse de l'université de Paris IX-Dauphine, 1992.

[7] I. Cohen, L.D. Cohen, N.Ayache, Using deformable surfaces to segment 3D images and infer differential structures, Computer vision, Graphics, and Image processing: Image understanding, 56(2), 242-263, sep 1992.

[8] L.D. Cohen On active contours models and balloons, Computer vision, Graphics, and Image processing: image understanding, 53(2), 211-218, March 1991.

[9] L.D. Cohen, E. Bardinet, N.Ayache, Surface reconstruction using active contour models, INRIA, rapport de recherche, 1992.

[10] L.D. Cohen, I. Cohen, Finite Element methods for active contour models and balloons from 2D to 3D, IEEE Transactions on Pattern Analysis and Machine Intelligence, PAMI-15(11), nov 1993.

[11] D. Euvrard, Résolution numérique des EDP de la physique, de la mécanique et des sciences de l'ingénieur, Masson 1988.

[12] C. Gout, An algorithm for C^k surface approximation with large variations, Int. J. of Computer Mathematics (79), no. 1, 111-131, 2002.

[13] C. Gout, S. Vieira-Testé, An algorithm for segmentation under interpolation conditions using deformable models. Int. J. Computer Math. (80), no. 1, 47–54, 2003.

[14] E. Laffon, Vallet C, Bernard V, Montaudon M, Ducassou D, Laurent F, Marthan R., A computed method for non invasive MRI assessment of pulmonary arterial hypertension, J Appl Physiol, in pressn 2003.

[15] E. Laffon, Laurent F, Bernard V, De Boucaud L, Ducassou D, Marthan R., Noninvasive assessment of pulmonary arterial hypertension by MR phase-mapping method, J Appl Physiol. 2001 Jun; 90(6): 2197-202, 2001.

[16] E. Laffon, Bernard V, Montaudon M, Marthan R, Barat JL, Laurent F., Tuning of pulmonary arterial circulation evidenced by MR phase mapping in healthy volunteers, J Appl Physiol. 2001 Feb; 90(2): 469-74, 2001.

[17] C. Le Guyader, D. Apprato, C. Gout, Using a Level Set Approach for Image Segmentation Under Interpolation Conditions., submitted, 2003.

[18] C. Le Guyader, Imagerie Mathématique: Théory et Applications, Thèse de Doctorat, en cours de rédaction, INSA Rouen.

[19] R. Malladi and Sethian, J.A., Image processing via level set curvature flow, Proceedings of the National Academy of Sciences, vol. 92 (15), 7046-7050, (1995).

[20] T. McInerney, D. Terzopoulos, Topology adaptive Deformable Surfaces for Medical Image Volume Segmentation, IEEE transactions on medical imaging, vol.18, no.10, 840, 1999.

[21] S. Osher, R. Fedkiw, Level Set Methods and Dynamic Implicit Surfaces, Springer Verlag, 2003.

[22] S. Osher, J.A. Sethian, Fronts propagating with curvature dependent speed: Algorithms based on Hamilton-Jacobi formulations, Journal of computational Physics 79, 12-49, 1988.

[23] M. Sonka, V. Hlavac, R. Boyle, Image Processing, analysis and machine vision , Chapman & Hall, 1993.

[24] D. Terzopoulos, A. Witkin, M. Kass, Symmetry seeking models for 3D object reconstruction , Proc. First International Conference on Computer Vision, London, England, IEEE, Piscataway, NJ, 269-276, 1987.

[25] S. Vieira-Teste, Représentation de structures géologiques à l'aide de modèles déformables sous contraintes géométriques, thèse de l'université de Pau et des pays de l'Adour, 1997.